YTUP

Journal of Thermal Engineering
https://jten.yildiz.edu.tr/
https://doi.org/10.47481/jten.0020

RESEARCH ARTICLE

Effect of tube arrangement on thermal and flow performance of tube bundle

Yogeshwari Kant[1], Rupesh Shah[2,*]

[1]Department of Mechanical Engineering, Sardar Vallabhbhai National Institute of Technology, Surat, Gujarat, 395007, India
[2]Department of Mechanical Engineering, Sardar Vallabhbhai National Institute of Technology, Surat, Gujarat, 395007, India

Abstract

The design of tube bundle arrangements strongly influences the thermal performance and pressure drop in compact heat exchangers, especially in low-Reynolds number applications where efficiency is critical. In this study, numerical analysis of the effect of unconventional tube bundle arrangements on heat transfer and flow characteristics was conducted, and their performance was compared with that of a conventional arrangement. Three different tube arrangements: diamond (9 tubes), staggered (13 tubes), and serpentine/sinusoidal (15 tubes) are considered for $1026 \leq Re \leq 10268$. Two-dimensional, steady, incompressible, thermally coupled flow analysis is performed using the commercial CFD tool ANSYS Fluent. Turbulence is modelled using the SST k-ω turbulence model. The streamline pattern over tube bundle arrangement reveals that the flow structure in the vicinity of the tubes is altered by the tube arrangement and the flow velocity. The diamond-shaped configuration incorporates a tubular arrangement that diverts the incoming flow while maintaining a low pressure drop. Staggered and serpentine tube arrangements force air to flow through the passages created by arranging the tubes in the bundle. Higher turbulent kinetic energy (TKE) and a higher number of tubes in these arrangements enhance heat transfer, at the cost of increased pressure drop. Over the range of Reynolds numbers considered, the serpentine arrangement exhibits an approximately 3% higher average Nusselt number Nu_{avg} (than the other two arrangements. The serpentine arrangement has three tubes in each row. In a serpentine arrangement, higher turbulent kinetic energy (TKE) and greater heat transfer area facilitate increased heat transfer $(\dot{Q})$. At low Re =1026, the serpentine arrangement provides a 39% higher heat transfer rate for the same pressure drop compared to the staggered arrangement, whereas the diamond arrangement yields 14% lower heat transfer rate. At higher Re, the performance of the serpentine arrangement is offset by a larger pressure drop, and the diamond arrangement is superior. The performance parameter, Pi, (ratio of $\dot{Q}$ and the pumping power) for the serpentine tube arrangement is high at low Re and comparable at higher Re whereas for the diamond layout, Pi remains almost constant throughout the range of Re. The serpentine arrangement outperforms other configurations in achieving a higher heat transfer rate and an optimal pressure drop. The novelty of this work lies in investigating the biomimetic serpentine (sinusoidal) and diamond-shaped tube arrangements, which are relatively unexplored compared to conventional inline or staggered tube banks.

Keywords: Tube arrangement, crossflow, heat transfer augmentation, pressure penalty, performance index

Cite this article as: Kant, Y., & Shah, R. (2026). Effect of tube arrangement on thermal and flow performance of tube bundle. Journal of Thermal Engineering, 12(3), 2–13. https://doi.org/10.47481/jten.0020

1. Introduction

Flow over the heated surfaces of a tube/fin bank in a heat exchanger is a primary area of study in heat transfer. Maximum heat transfer, and low-pressure drop are the two main objectives of heat transfer studies. These two objectives are inherently paradoxical. Enhancement of heat transfer can be achieved by increasing the number of tube/fin rows, choosing a staggered rather than an inline tube arrangement, and increasing the approach velocity of the fluid. To minimize pressure-drop in tube/fin bundles, tubes should be arranged such that they offer the least resistance to fluid flow. The optimal heat transfer and low-pressure drop characteristics of tube/fin bundle arrangement are of prime importance in thermal engineering because of their wide applications in heat exchangers, compact coolers, and energy exchange systems.

Numerous researchers have explored various aspects, including flow regimes, tube shapes, flow oscillations, turbulence and material properties to investigate the thermal and flow charac-

*Corresponding Author
E-mail Adress: rds@med.svnit.ac.in

Submitted: 28 May 2025; **Accepted:** 9 November 2025

This paper was recommended for publication in revised form by Editorin-Chief Ahmet Selim Dalkılıç

teristics of fluids exchanging heat with impermeable surfaces. These provide a vital understanding of the impact of flow, fluid, and geometrical parameters on the thermal and hydraulic performance of heat-exchanging systems. Low-Reynolds number applications have attracted attention because of their relevance to compact heat exchangers.

Studies by Yang et al. [1] and Nuntaphan et al. [2] elucidate the thermal performance and flow dynamics under these conditions, emphasizing the importance of geometric optimization for maximizing efficiency. Sahiti et al. [3] performed a comparative analysis of in-duct flow arrays with various pin cross-sections, highlighting the trade-offs between heat transfer enhancement and pressure drop. Six pin cross-sections were numerically investigated to identify the optimal fin shape that maximizes heat transfer while minimizing pressure drop. The analysis indicated that an elliptical section provides optimal performance under the same conditions. Liu et al. [4] and Zhou and Catton [5] extended this by numerically and experimentally investigating pin-fins with diverse cross-section shapes, including rectangular, elliptical, and circular designs. They also confirm the optimal performance of the elliptical shape compared with other shapes. Inducing flow oscillations in the approaching fluid is one way to increase heat transfer from tube surfaces. Jeng et al. [6] explored oscillating fluid flows through pin-fin arrays, emphasizing the role of oscillations in enhancing thermal performance. Flow oscillation enhances heat transfer performance under specific flow bypass conditions. Solomon and Gollub [7] investigated the thermal boundary layers in turbulent convection, revealing how recirculating flows contribute to higher heat flux transfer. They reported that turbulent convection is affected by large-scale flows near and within the boundary layers. Pottebaum and Gharib [8] investigated the effect of oscillatory flows around heated circular cylinders. Heat transfer enhancement was found to be strongly dependent on synchronization with harmonics of the natural shedding frequency, the cylinder wake mode, and the cylinder transverse velocity.

Staggered and inline tube/fin arrangements alter the flow regime in the vicinity of tube/fin surfaces. This change in flow regime affects flow and heat transfer characteristics. Staggered and inline configurations have been studied by many researchers for their impact on flow behaviour and thermal efficiency. Maji et al. [9] conducted numerical investigations on staggered and inline perforated pin-fin arrangements. Staggered layouts exhibit superior due to enhanced turbulence near heat transfer surfaces. Pati et al. [10] further confirm these findings. Reduced thermal resistance in staggered arrays at low-Reynolds numbers was observed. Material properties also play a crucial role in determining heat transfer characteristics. Peng et al. [11] analysed heat transfer and pressure drop characteristics of flat finned tube bundles with various fin materials. Thermal conductivity and material-specific properties significantly affect heat transfer characteristics. A hybrid approach that combines experimental and computational studies is advantageous for in-depth analysis of a limited number of cases. Adhikari et al. [12] reported an experimental and numerical study of forced convection heat transfer from rectangular fins at low-Reynolds numbers. Shorter fin channels were more effective at heat transfer than longer ones. Kamde and Dingare [13] carried out a combined numerical and experimental investigation of plate fin heat sinks and plate pin fin heat sinks having circular cross-section pin over a vertical base. For an inline arrangement, circular pin fins show that fin density and fin spacing have an appreciable influence on heat transfer characteristics. Innovative geometries and tube arrangements, such as serrated and sinusoidal fins, have been explored to enhance performance. Zhang et al. [14] studied the resistance characteristics of micro pin-fins fabricated for different shapes. Variation in thermal and hydraulic performance was noted. The pressure drop of the elliptical micro pin-fin is minimal compared with that of the other two pin-fin shapes (diamond and circular) at high Reynolds numbers. Gupta et al. [15] obtained the Nusselt number and friction factor by varying the system parameters as depth and pitch of the dimples, for inline and staggered arrangements. The inclusion of a dimple has been reported to improve heat transfer characteristics. Wei et al. [16] investigated a partially serrated finned tube bank. It was reported that with such geometries, heat transfer rates improve significantly while incurring acceptable pressure-drop penalties. Kawaguchi et al. [17, 18] explored spiral and serrated fin configurations for heat transfer analysis. It was concluded that these types of fins were more effective in turbulent flows. Deeb [19] investigated the influence of drop-shaped pin-fins on the thermal behaviour and flow characteristics of finned tubes. Drop-shaped fins enhanced heat transfer while incurring relatively small pressure penalties. Şahnali et al. [20] explored numerically the heat transfer and pressure drop of a wavy fin and Kammtail tube condenser. Reported results indicate that wavy fins exhibit improved heat transfer and a lower pressure penalty.

Zhao et al. [21, 22] studied the effect of tube arrangement on falling film heat transfer. Tube positioning plays an important role in fluid distribution and heat transfer. They studied turbulent falling films in horizontal tube bundles with different tube orientations. Square, rotated-square, triangular and rotated-triangular tube layouts affect turbulence and heat transfer. Jiang et al. [23, 24] investigated the impact of pulsating flow conditions and fin pitch-to-diameter ratios on heat transfer characteristics of the tube bundle. The study concluded that oscillation improves heat transfer. Tang et al. [25] examined variable direction twisted-oval tube (VDTOT) bundles. Compared to the circular tube, the VDTOT arrangement enhances heat transfer for the same pumping consumption due to the three-dimensional vortex mode. Zhou et al. [26] compared the performance of inline, column staggered and row staggered arrangements of tubes in H-type finned tube heat exchangers. It was concluded that the row-staggered tube arrangement outperforms the column-staggered and inline tube arrangements.

Flow acceleration, flow turbulence, flow oscillations, tube shape, rotating or oscillating tube/fin, flow re-circulation in the boundary layer region, tube arrangements, and wavy and dimpled fins are various means by which the heat transfer characteristics of the fin/tube surface can be augmented. To take advantage of many of these ap-

proaches, a specific requirement must be met. Flow oscillation, flow turbulence, rotating or oscillating tube and flow recirculation in the boundary layer region may require additional energy input. Fabrication of a peculiar fin shape may invite additional costs. Staggered and in-line tube/fin arrangements are the most popular and widely used for heat exchange in industry. Thus, a novel tube arrangement is needed to achieve optimal heat transfer with minimal pressure penalty.

The primary objective of the present study is to develop a tube arrangement for maximum heat transfer with an optimum pressure penalty for low-Reynolds number applications, due to its relevance in compact crossflow heat exchangers. Most previous studies have focused on conventional in-line or staggered pin-fin arrangements; however, present work numerically analyses the diamond and serpentine tube arrangements and compares them with the staggered configuration. The diamond and sinusoidal/serpentine arrangements are inspired by biomimicry, as many animals such as, fish and reptiles, exhibit wavy or curved geometries that reduce drag and enhance transport efficiency. A two-dimensional numerical analysis is performed over a range of approach velocities. Approach velocity varies between 1 m/s and 10 m/s. The results are presented in terms of heat transfer and pressure drop across the channel, which allows a fair comparison between the geometries. This study contributes to the literature by demonstrating the effectiveness of serpentine (sinusoidal) and diamond arrangements of pin-fins as compared with the conventional staggered pattern usually used in compact heat exchangers.

2. Geometry of tube bundle

In forced convection over a tube bundle, heat is exchanged across an impermeable surface separating hot and cold fluids. For a constant temperature difference between the hot and cold fluids, the rate of heat exchange is primarily governed by the level of turbulence in the vicinity of the tube surface. Increasing turbulence on the inner surface of the tube is not economically affordable. Passive methods and suitable tube arrangements can augment turbulence more efficiently on the outer surface of the tube. When tubes are inserted into the flow of gas, they reduce the available flow area and thereby increase resistance to flow. This requires greater pressure to overcome higher flow resistance. If tubes in a tube bundle are arranged such that they tear off the approaching fluid stream rather than pushing it, the flow resistance is reduced.

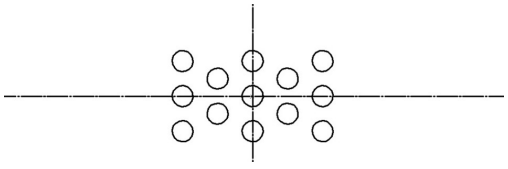

(a): Diamond arrangement

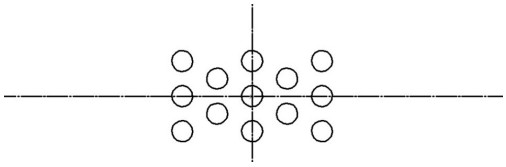

(b): Staggered arrangement

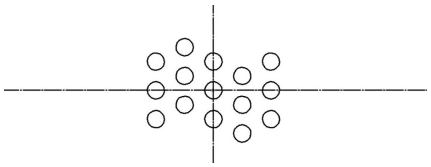

(c): Serpentine arrangement

Figure 1. Three different tube arrangements

Figure 1(a) shows a diamond-shaped tube arrangement. In this setup, there are 5 rows of tubes. The third row has a maximum three tubes. On both upstream and downstream sides of the third row, the number of tubes in each successive row is decreasing by one. In this arrangement, the flow is gradually exposed to the larger number of tubes as the fluid moves from the first row to the third row. After the third row, the number of tubes per row decreases. This increases the area available for flow. In five row diamond arrangement, nine tubes are incorporated. A staggered arrangement of tubes is presented in Figure 1(b). A staggered arrangement is a modified version of the diamond arrangement. If additionally, one tube is considered above and below for the 1^{st} and the 5^{th} row tube of the diamond tube arrangement, then the modified geometry represents a staggered tube arrangement. A staggered, five-row tube arrangement comprises thirteen tubes. The third tube arrangement considered in the present work is depicted in Figure 1(c). This is referred as a serpentine arrangement of tubes. In comparison to the staggered one, here one tube is added in each 2^{nd} and 4^{th} row. In the 2^{nd} row tube is added on the top side, while in the 4^{th} row tube is added on the bottom. This feature arranges the tube series in a serpentine pattern. The serpentine pattern is highlighted by a dotted curve in Figure 1(c). The serpentine arrangement consists of fifteen tubes arranged in five rows. For all arrangements, a tube with a diameter of 15 mm and longitudinal and transverse tube pitches of 25 mm is considered.

3. Domain and flow modelling

Following assumptions are made to carry out the flow modelling:

1. The flow is steady and incompressible.
2. No-slip boundary condition at walls.
3. Top and bottom walls are adiabatic.

The present two-dimensional numerical study requires flow and thermal analysis of the fluid as it passes over tube bundles. Sufficient upstream and downstream domain lengths ensure effective predic-

tion of flow physics and thermal characteristics. The tube bundle length, measured between the centre of the first row and the centre of the fifth row, along the flow direction, is 100 mm. This is the same for all three cases. The computational domain is extended up to 150 mm upstream of the centre line of 1st row of tubes. Similarly, the outlet boundary of the domain is considered at 150 mm downstream of the centre line of the 5th row of tubes. The domain extends 100 mm on either side of the horizontal axis of the tube bundle. The computational domain of the present study is shown in Figure 2. The left vertical boundary of the domain is assigned a velocity-inlet boundary condition. The right vertical edge is considered a pressure outlet. The top and bottom edges of the domain are assigned adiabatic wall conditions. All tube surfaces are treated as walls and are maintained at a constant temperature of 353 K.

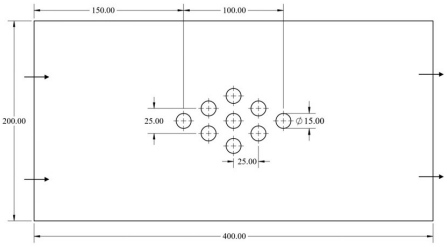

Figure 2. Computational domain

Predicting heat transfer associated with fluid flow requires solving the continuity, momentum, and energy equations. For the range of inlet velocities considered, the flow regime remains incompressible. Two-dimensional steady, incompressible, thermally coupled flow analysis is done using the commercial CFD tool ANSYS Fluent. Time-averaged governing equations as given in standard CFD literature [28] are:

Continuity equation:

$$\frac{\partial U}{\partial x} + \frac{\partial V}{\partial y} = 0 \quad (1)$$

x-momentum equation:

$$U\frac{\partial U}{\partial x} + V\frac{\partial U}{\partial y} = -\frac{1}{\rho}\frac{\partial P}{\partial x} + \upsilon\left(\frac{\partial^2 U}{\partial x^2} + \frac{\partial^2 U}{\partial y^2}\right) + \left(\frac{\partial}{\partial x}\tau_{xx} + \frac{\partial}{\partial y}\tau_{xy}\right) + S_x \quad (2)$$

y-momentum equation:

$$U\frac{\partial V}{\partial x} + V\frac{\partial V}{\partial y} = -\frac{1}{\rho}\frac{\partial P}{\partial y} + \upsilon\left(\frac{\partial^2 V}{\partial x^2} + \frac{\partial^2 V}{\partial y^2}\right) + \left(\frac{\partial}{\partial x}\tau_{yx} + \frac{\partial}{\partial y}\tau_{yy}\right) + S_y \quad (3)$$

Energy equation:

$$U\frac{\partial T}{\partial x} + V\frac{\partial T}{\partial y} = \alpha\left(\frac{\partial^2 T}{\partial x^2} + \frac{\partial^2 T}{\partial y^2}\right) + S_e \quad (4)$$

where U and V are the x and y components of the average fluid velocity, respectively. P denotes pressure, is the kinematic viscosity, T is the temperature, α is the thermal diffusivity, τ is the Reynolds stress, and S_x, S_y, S_e are the source terms for the x-momentum, y-momentum, and energy equations, respectively. Reynolds stresses are modelled using the SST k-ω turbulence closure model. In this study, the SST k-ω turbulence model is chosen because it is suitable for flows involving separation, recirculation, and strong near-wall effects, which are dominant in pin-fin heat transfer problems. The SST k-ω model can accurately capture boundary-layer development and transition to turbulence because its formulation is superior to that of the standard k-ε model. It blends the strengths of both the k-ε (in the free stream) and the k-ω (near the wall) models, providing better predictions of heat transfer and pressure drop.

3.1. Discretization and boundary conditions

The meshing capabilities of ANSYS are used to discretize the computational domain into an assembly of subdomains with known shapes. A sufficiently small grid is selected to generate the mesh. Edge sizing is applied specifically around the tube walls, having 90 cell divisions. This creates a fine mesh capable of capturing hydrodynamic and thermal boundary-layer phenomena occurring near the walls with reasonable accuracy.

The boundary conditions applied to the models are given in Table 1 below:

Table 1. Boundary Conditions

Boundary condition	
Fluid (air) density	1.225 kg/m^3
Fluid entering velocity	Range of 1-10 m/s
Temperature of entering fluid	300 K
Turbulent Intensity	5 %
Walls of domain	No-slip condition
Wall temperature of fins	353 K
Pressure at outlet	0 Pa (gauge pressure)
Method of solution	Coupled
Advection scheme for discretizing governing equations	Second Order Upwind
Convergence criteria for all equations	10^{-6}

3.2. Grid independence

Grid independence is a vital aspect of numerical study. Grid independence is conducted to ensure that grid refinement does not alter the results. To achieve grid-independent results, simulations are performed using three mesh sizes for the staggered tube arrange-

ment. The average Nusselt number of the tube bundle is used as a grid sensitivity parameter. The study is conducted at a maximum fluid velocity of 10 m/s. Three different minimum cell sizes, the total number of elements in the domain, and the corresponding average values of the Nusselt number (Nu_{avg}) are tabulated in Table 2.

Table 2. Data of grid independence study

Minimum cell size	No. of elements	Nu_{avg} of tube bundles
1 mm	81859	67.15
0.8 mm	125217	65.92
0.6 mm	219652	65.99

The comparison of the data presented in Table 2 indicates that by reducing the cell size from 1 mm to 0.8 mm, the total no. of elements in the domain increases by 53% relative to the 1 mm cell size. The average value of Nu_{avg} decreases from 67.15 to 65.92. The reduction in Nu_{avg} due to grid refinement is approximately 1.86%. When the minimum cell size is further reduced to 0.6 mm, the total number of elements in the domain becomes 219,652. The average Nu_{avg} values for cell sizes of 0.8 mm and 0.6 mm are comparable. The deviation of for these cases is less than 0.02%. Thus, the total number of 125,217 elements with a minimum cell size of 0.8 mm constitutes a grid-independent case. For further numerical analysis, the domain is discretized using a minimum cell size of 0.8 mm.

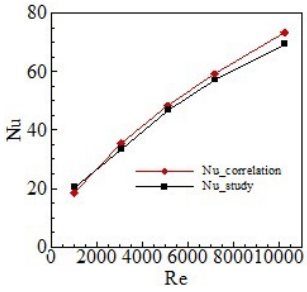

(a)

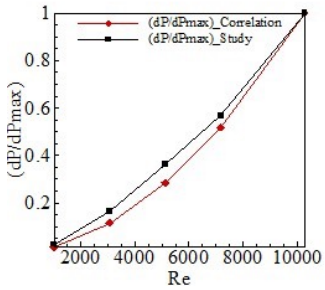

(b)

Figure 3. Validation of results with correlations

4. Results and discussion

Figure 3(a) compares the Nu_{avg} variation obtained from the present study to that obtained from the empirical correlation proposed by Zukauskas [28]:

$$Nu_{avg} = 0.35F\left(\frac{S_T}{S_L}\right)^{0.2} Re_D^{0.6} Pr^{0.36} \left(\frac{Pr}{Pr_s}\frac{Pr}{Pr_s}\right)^{0.25} \quad (5)$$

where S_T is the transverse pitch, S_L is the longitudinal pitch between tube centres, F is the correction factor for the number of tube rows < 16 (for 5 rows, F = 0.93) which can be obtained from the above reference, Pr is the Prandtl number, and Pr_s is the Prandtl number at temperature T_s, which is the temperature of the tube walls. Trends in variation are comparable. The present study underpredicts the Nu_{avg} value relative to the empirical correlation. The deviation of Nu_{avg} is smaller at low-Re values and is below 6% at higher-Re values.

The pressure drop obtained in the staggered arrangement is compared with the pressure drop calculated from the following correlation [29]:

$$dP = N_L f \chi \frac{\rho V_{max}^2}{2} \quad (6)$$

where N_L is the number of rows, f is the friction factor, and χ is the correction factor. f and χ can be obtained from available charts [29]. The numerical value of the pressure drop is normalised to the maximum pressure drop corresponding to the maximum velocity (10 m/s). Pressure drops calculated from the correlation are normalised by the maximum pressure penalty at a velocity of 10 m/s. A comparison of these normalised pressure drops is shown in Figure 3(b). The trends in pressure drop are comparable. The maximum deviation is below 12%. The present case overpredicts because of differences in geometrical configurations and domain size. In the present case, longitudinal and transverse tube pitches are the same, whereas in the correlation, the unequal. Another reason might be that the present simulation domain is 2-D, while the correlation experiments were performed over a 3-D domain.

These indicate that the quality of domain discretization, the schemes used for discretizing governing differential equations, and the models used for representing physical phenomena are in order. Further analysis is carried out using a grid-independent size and validated methodology. Results are compared in terms of overall flow behaviour, streamline patterns, turbulence levels, pressure variations, local and average Nusselt numbers and gross heat transfer performance. These results are presented and discussed in the following sections.

Note: Sample calculations for Nu_{avg}

The area-weighted average static pressure at the inlet and outlet are obtained from the ANSYS Fluent simulation report. Hence, the pressure drop is calculated as $P = P_{in} - P_{out}$

Heat flux transferred across the walls is also extracted frWom the report and averaged over the walls. These values of are used to calculate the convective heat transfer coefficient (h) on the walls by using the formula $h = \frac{\dot{q}}{(T_{wall} - T_{fluid})}$

Hence, the Nusselt number can be obtained using , where D is the diameter of the circular fin (15 mm) and k is the thermal conductivity of the material.

Note: Maximum velocity calculation for the channel

Since both the biomimetic arrangements, diamond and serpentine/ sinusoidal, are variations of the staggered pattern, in which the circular fins are arranged alternately, the maximum velocity can be calculated using the following equation [29]:

$$v_{max} = \frac{S_T}{2(S_D - D)}v, \quad (7)$$

where S_T is the transverse pitch, S_D is the diagonal pitch of the pattern and D is the diameter of fins. These values are equal for all three arrangements S_T = 25 mm, $S_D = 25\sqrt{2}$ = 35.3 mm and D = 15 mm.

Hence, using the above relation, we obtain the common maximum velocity as ≈ 0.62. The maximum velocity will be used to calculate the Reynolds number in each case to evaluate Nu_{avg} .

4.1. Effect of tube arrangements on flow structure

Fluid flow in a confined domain maintains its flow regime in the absence of obstructions. An obstruction forces the flow to divert and generates a downstream wake. The degree of diversion and the shape and strength of the wake zone are determined by the shape and size of the obstruction and by flow velocity. In the present case, three different tube arrangements are investigated numerically. In a diamond-shaped tube arrangement, the number of tubes increases gradually to three and then decreases to one. In this typical arrangement, the flow is gradually exposed to a larger number of tubes in series. This specific tube pattern avoids high flow resistance in the first row of tubes. There is only one tube in the 1st row, two tubes in the 2nd row and three tubes in the 3rd row, forming a structure like arrowhead. This structure facilitates tearing of the airflow rather than opposing it. This can be observed from the streamline patterns presented in Figures 4(a) and 4(b) for air flow velocities of 5 m/s and 10 m/s. Initially, the flow impinges on the single tube in the first row, and as it moves along the tube walls, a thin boundary layer begins to develop. A relatively small wake region forms at the rear of the tube, where flow recirculation is limited. On the other hand, at higher velocities, the fluid interacts with the tube more vigorously, causing rapid boundary layer formation. The flow separation also occurs earlier, and the wake region is larger than that of the low velocity case. This can be observed by comparing the streamline patterns for the 5 m/s and 10 m/s cases, as shown in Figures 4(a) and 4(b).

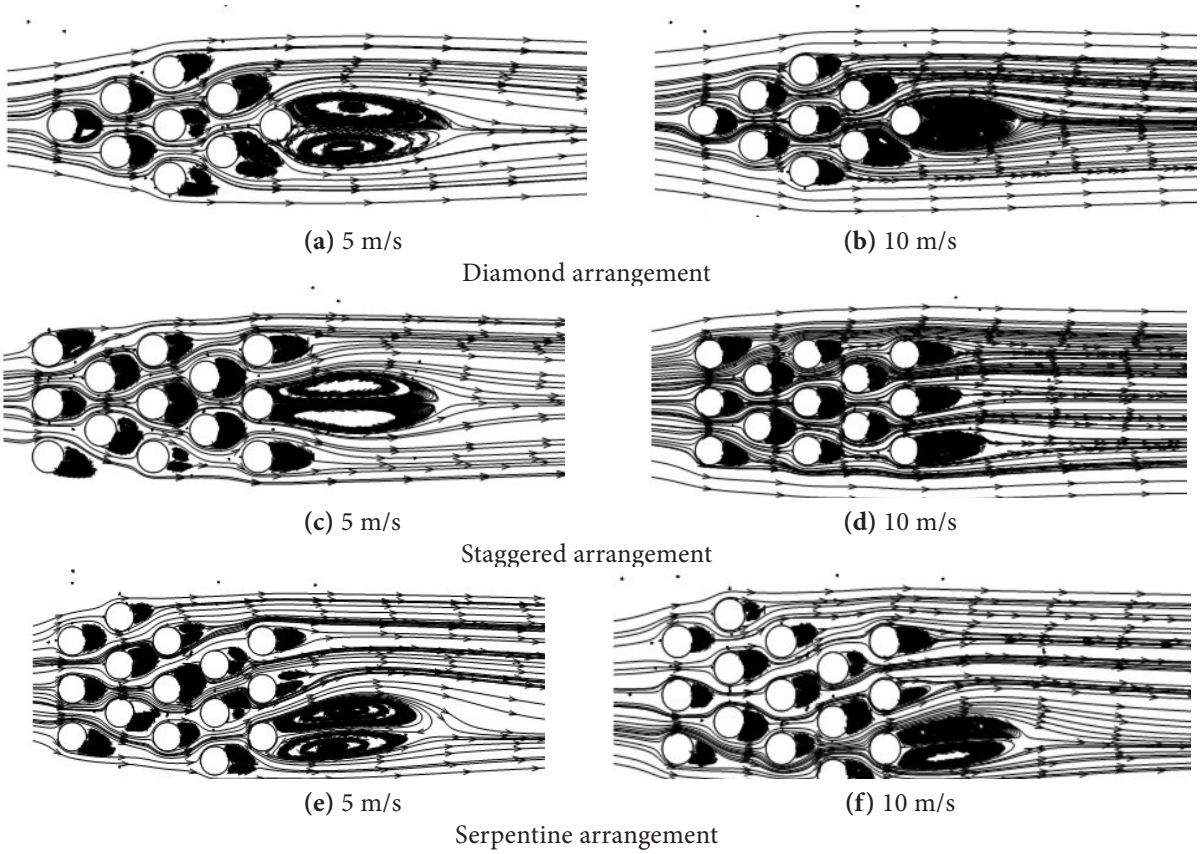

(a) 5 m/s **(b)** 10 m/s

Diamond arrangement

(c) 5 m/s **(d)** 10 m/s

Staggered arrangement

(e) 5 m/s **(f)** 10 m/s

Serpentine arrangement

Figure 4. Streamline pattern over tube arrangements

As the fluid flows to the next row, it splits into the two tubes. The wake region on the leeward side of the second row of tubes is larger than that of the first row. This indicates that a larger volume of fluid remains trapped in the wake zone. Because the third row contains the largest number of tubes, the flow is more turbulent. The middle tube in the third row receives fluid that flows from the tubes of the first and second rows. The other two tubes at either end primarily receive the fresh fluid stream. The wake region of the third-row tubes is slightly inclined because only two tubes are present in the fourth row. The angle of inclination is larger at a fluid velocity of 10 m/s than at 5 m/s. In the next row, there are two tubes again. They receive low-momentum fluid from the gap between two pairs of tubes in the previous row. The wake regions behind the tubes in fourth row are significantly larger than those in earlier rows. These wake zones are little deformed by the free stream flow and due to the presence of the tube in the 5^{th} row. In the last row, the tube receives fluid that has moved through the gaps between pairs of tubes in the third and fourth rows. The wake on the leeward side of the last tube is larger and extends over a longer distance. This is evident from the streamline pattern as shown in Figure 4(a). Comparison of streamline patterns at 5 m/s and 10 m/s reveals a larger wake zone at the lower velocity than at the higher velocity. At low velocity, less fluid with low momentum flows over the tubes. This facilitates the growth of the wake zone. At high velocity, a greater mass of fluid with high momentum flows over the tubes. This restricts the growth of wake zones behind tube surfaces.

The staggered tube arrangement includes two additional tubes in each 1^{st} and 5^{th} row. As a result, the flow shows greater disturbances in the first row than in the diamond arrangement. The flow regime exhibits a symmetric separation zone around the tubes, owing to the greater number of tubes in the first row. Longer wake region forms compared with those in the diamond arrangement. The wake region formed behind the tubes extends to the tubes in the next row. At 5 m/s, the wake zone is longer than in the diamond case. This can be observed in the streamline distribution presented in Figure 4(c). This is because in a staggered arrangement the mass and momentum of fluid flowing over central tubes or through the tube pitch in the centre are lower at low velocity. This low-momentum fluid is unable to restrict wake development and growth. A relatively large fluid mass with higher momentum flows through the same area at 10 m/s, restricting the formation of the wake zone. Thus, a smaller wake is observed at higher velocity.

In a serpentine arrangement, extra tubes are added to the second and fourth rows, maintaining the staggered pattern. Adding tubes to the second row significantly alters the flow regime. The same can be observed by comparing the streamline patterns near the 2^{nd} row in the staggered and serpentine arrangements. An extra tube in the 4^{th} row alters the flow regimes for the tubes 5^{th} row, which are in the wake zone of that extra tube. A larger, longer wake zone forms because of the extra tube in the fourth row. This is evident when comparing the streamline patterns of the staggered and serpentine arrangements. The presence of larger and longer wakes on the leeward side of the tube in the last row is due to low-momentum fluid approaching the 5^{th} row tubes due to the presence of an additional tube present ahead of it.

4.2. Temperature distribution over tube arrangements

For cases tested numerically in the present study, the tube surface is maintained at a constant temperature of 353 K. Figures 5(a) and 5(b) present temperature contours in the flow domain for the diamond arrangement. Comparison of these contours for the 5 m/s and 10 m/s cases indicate that the thermal boundary layer at 5 m/s is thicker than at 10 m/s. At low velocity, fluid has lower turbulence and lower momentum than at high velocity. Low-momentum fluid exhibit high temperature gradients. This results in a larger effective area over which the fluid is exposed to a high temperature tube surface. This can be observed as a larger area of the flow domain over which the temperature varies from minimum to maximum. At higher velocity, the thermal boundary layer is thin, which restricts the region of temperature variation to the vicinity of the tube surfaces and the wake zone behind the tube. As the fluid continues to flow through the tube space and over tubes in different rows, it becomes heated due to heat transfer from the tube surfaces. Also, the size of the wake zone increases. These combined effects result in a reduced heat absorbing capacity and a low rate of heat transfer to the fluid as it flows over successive tubes. This establishes a wider thermal boundary layer in the direction of fluid flow as air moves from the first to the last row of tubes.

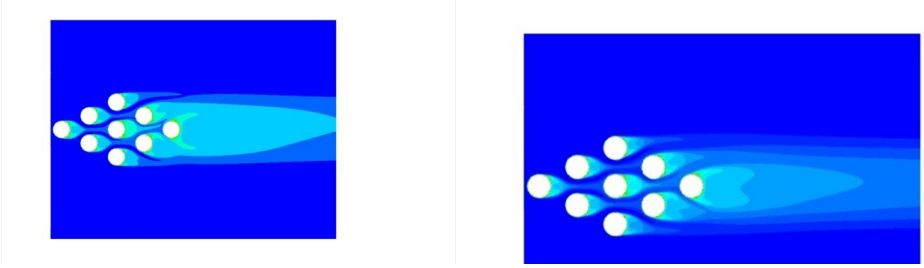

(a) 5 m/s **(b)** 10 m/s

Diamond arrangement

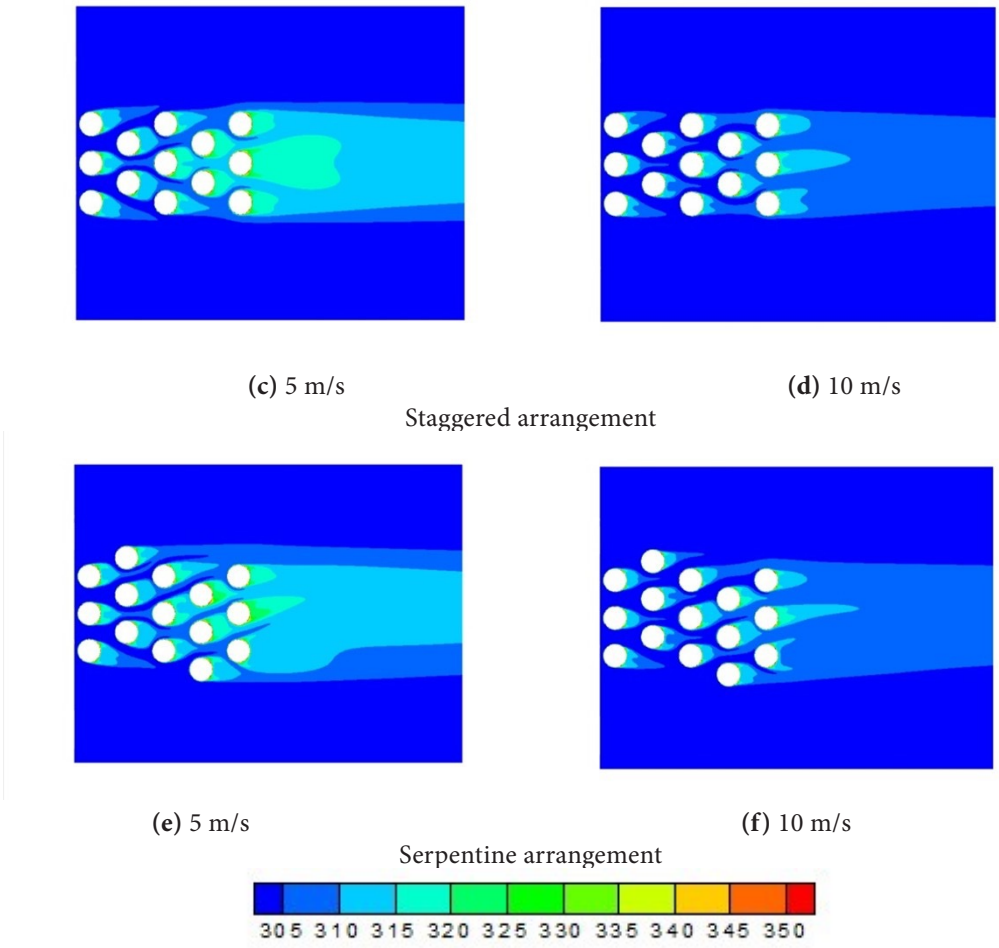

Figure 5. Temperature (K) contours over tube arrangements

In a staggered tube arrangement, the first row of the tube bundle contains two additional rows of tubes compared with the diamond arrangement. Due to this, air flowing through the tube gaps is accelerated. This can be verified by the convergence of streamlines, as shown in Figure 4. Flow acceleration over tubes increases fluid momentum and turbulence. A relatively larger wake zone behind the tube surface in a staggered arrangement results in a larger heat-trap zone. This can be observed by comparing the temperature contours of the diamond and staggered arrangements at the same velocity. The size of the wake zone decreases at higher velocity. This significantly compresses the temperature zone near the tube surface. The same can be observed by comparing the contours of the temperature distribution presented in Figures 5(c) and 5(d).

The serpentine arrangement contains an additional tube in both the second and fourth rows. This alters the flow structure near the additional tube in the second row. In the fourth row, the flow regime near and behind the additional tube is also altered. Flow obstruction and acceleration due to the additional tube in the second and fourth rows alter the streamline pattern and the shape and size of the wake zone, as shown in Figure 4. This modification of the flow regime due to increased momentum and turbulence restricts the spread of high temperature to the region near the tube surface. This can be observed by comparing the temperature contours of staggered and serpentine arrangements. An increase in velocity from 5 m/s to 10 m/s produces effect like those of staggered and diamond tube arrangements.

4.3. Row-wise variation of Nusselt Number and heat flux potential

The row-wise variations of the average Nusselt number and heat-flux potential (number of tubes × heat flux) at 10 m/s are presented in Figure 6(a) and 6(b), respectively. Figure 6(a) depicts that the average value of in the diamond layout increases from 1st to 3rd row and decreases thereafter. Maximum value of row-wise average is reported for the 3rd row. Turbulence reaches a maximum in the vicinity of the tubes in the third row of the diamond layout. This is evident from the contours of turbulent kinetic energy (TKE) shown in Figure 7. Contours of TKE indicate that TKE is maximal near the

3rd row and minimal near the last row in the diamond layout. The presence of two tubes in each of the 2nd and 4th rows of the diamond arrangement results in higher TKE in the vicinity of tubes in the 3rd row. This facilitates a higher value of for the 3rd row of the tube. of the 3rd row is 6% and 33% higher in comparison to that of the 1st and last row of the diamond layout. For a constant temperature difference, the heat transfer rate is decided by and area. Figure 6(b) describes the row-wise variation of heat flux potential q_{avg_r} It is high in the third row and lower in the last row. For the third row, Nu_{avg_r} and the number of tubes is maximum. These results in highest q_{avg_r} for the third row.

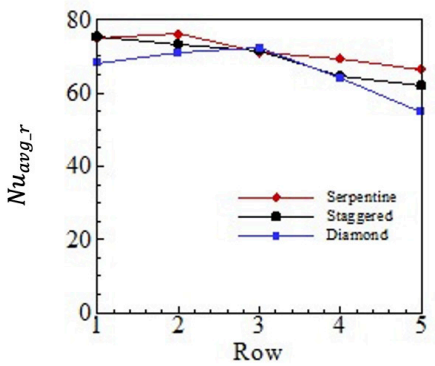

(a) Nu_{avg_r} variation

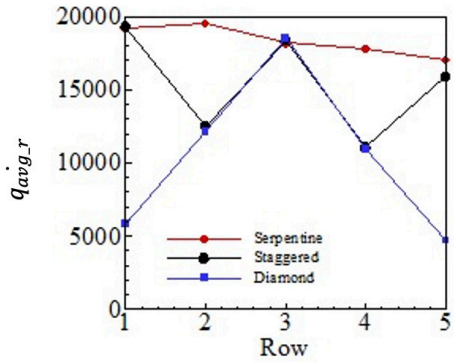

(b) Heat flux potential

Figure 6. Row-wise variation Nu_{avg_r} and q_{avg_r} at 10 m/s

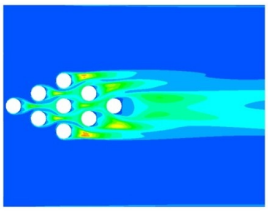

(a) Diamond arrangement

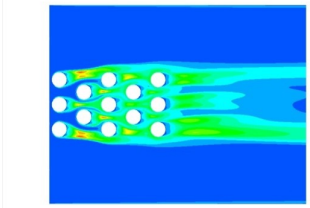

(b) Staggered arrangement

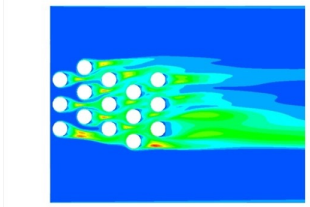

(c) Serpentine arrangement

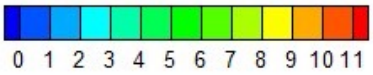

Figure 7. Variation of TKE (m2/s2) at 10 m/s

In staggered arrangement, the maximum value of Nu_{avg_r} and q_{avg_r} are observed for 1st row compared to 3rd row in case of diamond arrangement. Nu_{avg_r} values of 1st and 5th row of staggered arrangement is higher by 10% and 14 % respectively compared to that of diamond tube arrangement. Value of Nu_{avg_r} is reducing from 1st to 5th row of tube. This is because 1st row of staggered arrangement offers large resistance to incoming flow compared to that of the diamond arrangement. Contours of TKE plotted in Figure 7(b) indicate that the flow in the vicinity of tubes of 1st row has high TKE compared to tubes in other rows. Higher TKE with low air temperature ensures higher Nu_{avg_r} for 1st row. 1st row of staggered arrangement also causes acceleration of fluid as it passes through the tube gaps/pitches. This high-momentum fluid hits the tubes of the second row and generates additional turbulence. Higher turbulence near the 2nd and 3rd row of tubes assists the flow to absorb enough heat from tube surfaces and keep comparable with that of the 1st row of tubes. After the third row, high temperatures wake zones of preceding tubes extend up to successive tubes. This avoids the flow of low temperature air over tubes of the 4th and 5th row. Thus Nu_{avg_r} and q_{avg_r} decreases as shown in Figure 6(a) and 6(b). In both diamond and staggered arrangements, after 3rd row, turbulence decreases while air temperature increases. This reduces overall heat transfer and results in a low value of Nu_{avg_r} after 3rd row of tubes. In staggered arrangements heat flux potential of the 1st and 5th tubes is increased compared to the diamond arrangement. This is due to the increased convection area due to the consideration of two additional tubes in the 1st and 5th row. Heat flux values in the 2nd to 4th rows are comparable due to the identical number of tubes in rows.

For staggered and serpentine arrangement, Nu_{avg_r} and q_{avg_r} are comparable for 1st row of tubes. This can be observed from Figure 6. Tube arrangements in serpentine are like staggered, except for additional tubes in the 2nd and 4th rows. This additional tube in a specific row alters the flow regime and thermal characteristics of fluid flowing over tubes, specifically in the 2nd and 4th rows. The same can be observed by comparing streamline patterns, contours of temperatures and TKE as shown in Figures 4, 5 and 7 respectively. On the windward side, additional tube in the 2nd row receives a combination of low temperature air (in the upper half) and turbulent air with moderate temperature (in the lower half). Also wake zone of the additional tube in the 2nd row is smaller in the longitudinal and normal direction to the flow. Due to the combined effect of this, Nu_{avg_r} and q_{avg_r} for the tubes in the 2nd row increases and achieve highest value compared to other tube arrangements. Nu_{avg} and for 3rd row tube is comparable for all three arrangements due to the similarity in flow regime in the vicinity of the tubes of the 3rd row. In the 4th row, the addition of one more tube increases Nu_{avg} and q_{avg_r}. This can be observed by comparing the variation of Nu_{avg} and q_{avg_r} for staggered and serpentine arrangements. In a serpentine arrangement variation of Nu_{avg} and q_{avg_r} are more uniform compared to the other two tube arrangements due to the presence of an equal no of tubes in all the rows.

Figure 8 compares the Nu_{avg} variation against Re for three different arrangements. Nu_{avg} For all three arrangements increases with a rise in Re. At low Re, the diamond and serpentine arrangements are 20% higher Nu_{avg} compared to the staggered one. At all ranges of Re considered in the current study, serpentine arrangements reflect around 3% higher value of Nu_{avg} over the other two arrangements. This is due to the specific serpentine tube pattern, which increases TKE in the vicinity of the tube surfaces.

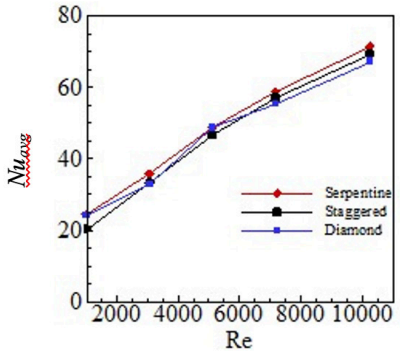

Figure 8. Nu_{avg} vs Re

4.4. Overall heat transfers and pressure penalty for tube arrangements

The thermal and flow performance of the tube bundle are judged by comparing the variation in the overall heat transfer rate $\dot{Q}$, and associated pressure penalty. Figure 9 shows how the heat transfer rate varies with Re for all three tube arrangements. For the specific tube arrangement, $\dot{Q}$ increases with increasing Re. Across the entire range of Re considered in the present study, the serpentine arrangement exhibits the highest Nu_{avg} among the arrangements. This is due to increased turbulence in the serpentine tube bundle caused by specific tube arrangements. The rate of rise of $\dot{Q}$ at low Re is higher than at high Re. At Re = 1026 (V = 1 m/s), the serpentine arrangement provides a 39% increase, and the diamond arrangement provides a 18% decrease, compared with the staggered arrangement. At Re = 10268 (V= 10 m/s), the serpentine arrangement exhibits 19% higher values, while the diamond arrangement exhibits 33% lower $\dot{Q}$ values compared to a staggered arrangement.

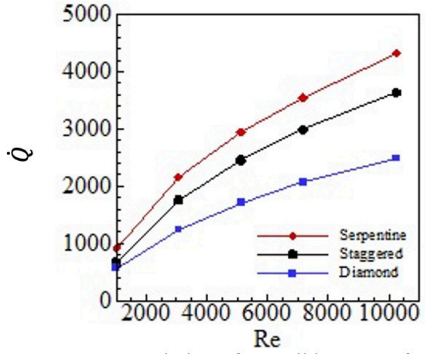

Figure 9. Variation of overall heat transfer

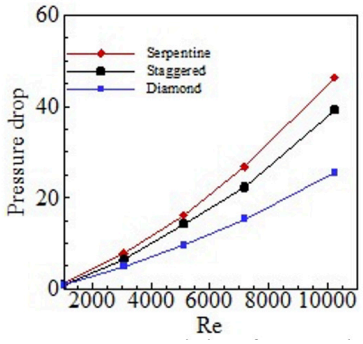

Figure 10. Variation of pressure drop

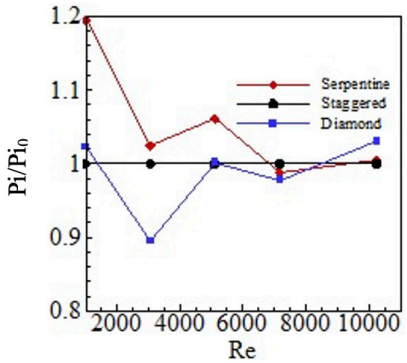

Figure 11. Variation of relative performance index

Enhancement of $\dot{Q}$ with Re comes at the cost of a higher pressure drop (-Δp). Figure 10 shows how the pressure drop varies with increasing Re for three different arrangements. The pressure drops increase exponentially with increasing Re. The serpentine arrangement exhibits the highest pressure drop at the same Re among all arrangements. This is due to the typical and maximum numbers of tube arrangements in this case. A larger number of tubes will reduce the flow area and increase flow resistance. This results in a higher-pressure penalty. At lower Re = 1026, the pressure drop is comparable across all three arrangements. The difference in pressure drop widens as Re increases. At Re = 10268, the serpentine arrangement requires an 18% higher pressure drop, and the diamond arrangement exhibits a 35% lower pressure drop compared to the staggered arrangement. Comparison of the variation of $\dot{Q}$ with -Δp reveals that better heat transfer can be obtained at the cost of a higher pressure drop. To arrive at a fair assessment of the tube bundle, the performance is evaluated by comparing the performance indices of different tube arrangements.

The performance index (Pi) is defined as the ratio of the heat transfer rate to the pumping power required to blow air over the tube bundle. Figure 11 describes the variation of the performance index with respect to staggered arrangement (Pi/Pi_0) for all three cases. Variation indicates that in all three arrangements, Pi decreases as Re increases. Both and -Δp are functions of Re. This is evident from the trends presented in Figures 8 and 10. For a given set of constraints, if Re is varied by changing only flow velocity, the trends indicate that Nu is a weak function of Re, whereas –Δp is a strong function of Re. Consequently, as Re increases, Pi decreases rapidly for Re up to approximately 3000. A further rise in Re reduces Pi, but the rate of reduction decreases because the rate of rise of –Δp changes. Among three arrangements, serpentine has a higher Pi at all levels of Re. The difference is larger at low Re values than at high Re values. At low Re, the serpentine tube bundle has 20% higher Pi than the staggered arrangement. The difference in Pi narrows to 5% when Re increases to 7000. After that, the Pi of all arrangements is comparable. Higher Pi for the serpentine arrangement at low Re values and up to Re = 7000 makes it an optimal choice for enhanced heat transfer with a moderate pressure drop.

5. Conclusion

Numerical analysis is carried out to investigate the thermal and flow performance of different tube arrangements. For diamond, staggered and serpentine tube arrangements, overall flow structure, temperature contours and heat transfer characteristics are compared for $1026 \leq Re \leq 10268$ The major conclusions of the present numerical study are:

1. Diamond tube arrangement $1026 \leq Re \leq 10268$ yields the lowest pressure drop (0.78 to 25.5 Pa), compared with the staggered arrangement (0.97 to 39.2 Pa); the sinusoidal arrangement has the highest pressure drop across the channel, ranging from 1.14 to 46.4 Pa. This means that the pumping power required is highest in a sinusoidal layout and lowest in a diamond pattern.
2. On the other hand, the diamond arrangement has the lowest heat transfer rate from the walls to the fluid ($571 \leq \dot{Q} \leq 2487$) compared with the staggered arrangement ($668 \leq \dot{Q} \leq 3636$), and the highest heat transfer rate in the sinusoidal arrangement ($922 \leq \dot{Q} \leq 4320$).
3. A serpentine tube arrangement provides greater uniformity of the Nusselt number and heat-flux across all rows of the tube bundle than diamond and staggered arrangements.
4. At a low Reynolds number of 1026 (V = 1 m/s), a serpentine arrangement provides a 39% higher heat transfer rate for the pressure drop compared to a staggered arrangement.
5. Variation of performance index Pi, for range of Reynolds numbers tested indicates that Pi for serpentine is greater than ($Re \leq 7000$) or comparable ($7000 < Re \leq 10268$) with staggered arrangement which allows us to conclude that sinusoidal/serpentine arrangement outperforms in terms of high heat transfer rate and pressure drop.
6. Consequently, serpentine or sinusoidal arrangement of pin-fins can be implemented in practice in compact heat exchangers, electronic cooling modules, and turbine blade cooling channels because such a layout disrupts flow uniformity and enhances local turbulence resulting in a greater rate of heat transfer.
7. The present study addresses the lack of research on unconventional biomimetic tube arrangements compared with the widely studied in-line and staggered configurations. However, further work, including experimental validation, could examine the microscale flow physics, vortex formation and turbulence characteristics generated by such arrangements.

Conflict of Interest

The authors declare that they have no competing interests.

Acknowledgement

No financial help is received from any agency.

Funding

No fund is received from any source to carry out present study.

Author Contribution

Yogeshwari Kant conducted parametric investigation, analysed the results, drafted manuscript and arranged data. Rupesh Shah conceptualized research work, derived methodology and supervised overall study, review and edited article.

Copyright and permission statement

All elements referred to as figures within this manuscript are original and newly created/generated.

References

[1] Yang, Kai Shing & Chu, Wei-Hsin & Chen, Ing & Wang, Chi-Chuan. (2007) Experimental Investigations on Airside Performance of Heat Sinks Having Pin Fin Configurations. Annual IEEE Semiconductor Thermal Measurement and Management Symposium. 208 - 212. https://doi.org/10.1109/STHERM.2007.352425

[2] Nuntaphan, A. & Kiatsiriroat, Tanongkiat & Wang, Chun-chang. (2005). Air side performance at low Reynolds number of crossflow heat exchanger using crimped spiral fins. International Communications in Heat and Mass Transfer. 32. 151-165. https://doi.org/10.1016/j.icheatmasstransfer.2004.03.022

[3] Sahiti, Naser & Lemouedda, A. & Stojkovic, D. & Durst, F. & Franz, E. (2006). Performance comparison of pin fin in-duct flow arrays with various pin cross-sections. Applied Thermal Engineering. 26. 1176-1192. https://doi.org/10.1016/j.applthermaleng.2005.10.042

[4] Liu, Z.G. & Guan, Ning & Zhang, C.W. & Jiang, G.L. (2015). The Flow Resistance and Heat Transfer Characteristics of Micro Pin-Fins with Different Cross-Section Shapes. Nanoscale and Microscale Thermophysical Engineering. 19. 221-243. http://dx.doi.org/10.1615/IHTC15.nmm.008946

[5] Zhou, Feng & Catton, Ivan. (2011). Numerical Evaluation of Flow and Heat Transfer in Plate-Pin Fin Heat Sinks with Various Pin Cross-Sections. Numerical Heat Transfer Applications. Part A: Applications. 107-128. https://doi.org/10.1080/10407782.2011.588574

[6] Jeng, Tzer-Ming & Tzeng, Sheng-Chung & Hsu, Wei-Ting & Xu, Guan-Wei. (2015). Flow Visualization and Heat Transfer Characteristics of Oscillating Fluid through Pin-Fin Array in a Rectangular Channel. Advances in Mechanical Engineering. https://doi.org/10.1155/2013/283830

[7] SOLOMON, TH & GOLLUB, JP. (1991). Thermal boundary layers and heat flux in turbulent convection: The role of recirculating flows. Physical Review A. 43. 6683-6693. https://doi.org/10.1103/PhysRevA.43.6683

[8] Pottebaum, Tait & Gharib, Mory. (2006). Using oscillations to enhance heat transfer for a circular cylinder. International Journal of Heat and Mass Transfer - INT J HEAT MASS TRANSFER. 49. 3190-3210. https://doi.org/10.1016/j.ijheatmasstransfer.2006.01.037

[9] Maji, Ambarish & Bhanja, Dipankar & Patowari, Promod. (2017). Numerical investigation on heat transfer enhancement of heat sink using perforated pin fins with inline and staggered arrangement. Applied Thermal Engineering. 125. https://doi.org/10.1016/j.applthermaleng.2017.07.053

[10] Pati, Biswaranjan & Sharma, Bishwajit & Palo, Ashutosh & Barman, Rabindra. (2018). Numerical investigation of pin-fin thermal performance for staggered and inline arrays at low Reynolds number. International Journal of Heat and Technology. 36. https://doi.org/10.18280/ijht.360235

[11] Peng, Y & Zhang, S & Shen, F & Wang, X & Yang, X & Yang, L. (2017). Numerical studies on heat transfer and pressure drop characteristics of flat finned tube bundles with various fin materials. IOP Conference Series: Earth and Environmental Science. 93. 012067. https://doi.org/10.1088/1755-1315/93/1/012067

[12] Adhikari, Rc & Wood, David & Pahlevani, M. (2020). An experimental and numerical study of forced convection heat transfer from rectangular fins at low Reynolds numbers. International Journal of Heat and Mass Transfer. 163. 120418. https://doi.org/10.1016/j.ijheatmasstransfer.2020.120418

[13] Kamde, Gaurav & Dingare, Sunil. (2017) Experimental and Computational Investigation of Forced Convection Analysis of Plate Circular Pin Fin Heat Sinks over Vertical base. Journal of The Institution of Engineers (India): Series C. 99. 1-10. https://doi.org/10.1007/s40032-017-0363-0

[14] Zhang, C. & Pu, L. & Jiang, G. & Guan, N. & Liu, Z.(2014). Resistance characteristics of micro pin fins with different cross-section shapes. Huagong Xuebao/CIESC Journal. 65. 2042-2048. https://doi.org/10.3969/j.issn.0438-1157.2014.06.013

[15] Gupta, Ayush & Kumar, Manoj & Patil, Anil. (2019). Enhanced heat transfer in plate fin heat sink with dimples and protrusions. Heat and Mass Transfer. 55. https://doi.org/10.1007/s00231-019-02561-w

[16] Wei, Hongyu & Cong, Tao & Jiang, Chen & Zhou, Wenxue & Bai, Bo. (2023). Heat Transfer Enhancement of Partially Serrated Twisted Finned Tube Bank. Heat Transfer Engineering. 44. 1-21. https://doi.org/10.1080/01457632.2022.2164682

[17] Kawaguchi, Kiyoshi & Okui, Kenichi & Asai, Toshihiro & Hasegawa, Yutaka. (2005). The Heat Transfer and Pressure Drop Characteristics of the Finned Tube Banks in Forced Convection (Effects of Fin Height on the Pressure Drop Characteristics). Heat Transfer—Asian Research. 35. 194 - 208. https://doi.org/10.1002/htj.20111

[18] Kawaguchi, Kiyoshi & Okui, Kenichi & Takaki, Yusaku. (2006). Effects of Flow around Fin on the Heat Transfer and Pressure Drop Characteristics of the Spiral Finned Tube Banks. Transactions of the Japan Society of Mechanical Engineers Series B. 72. 1310-1317. https://doi.org/10.1299/kikaib.72.1310

[19] Deeb, Rawad. (2024). The impact of drop-shaped pin-fins on the thermal and hydraulic characteristics of a finned tube. Physics of Fluids. 36. 75148. https://doi.org/10.1063/5.0218237

[20] Şahnali, Funda & Atayılmaz, Ş & Gemici, Zafer. (2024). Numerical analysis of the heat transfer and pressure drop of a wavy fin and Kammtail tube condenser: An investigative study. Case Studies in Thermal Engineering. 55. 104191. https://doi.org/10.1016/j.csite.2024.104191

[21] Chuang-Yao Zhao, Zhuo-Liang Yao, Di Qi, Wen-Tao Ji, An-Gui Li, Wen-Quan Tao. (2022). Numerical investigation of tube bundle arrangement effect on falling film fluid flow and heat transfer. Applied Thermal Engineering, Volume 201, Part B, 2022, 117828, ISSN 1359-4311. https://doi.org/10.1016/j.applthermaleng.2021.117828

[22] Chuang-Yao Zhao, Zhuo-Liang Yao, Di Qi, Wen-Tao Ji, Wen-Quan Tao. Hydrodynamics and thermal performance of turbulent falling films through horizontal tube bundles. International Journal of Multiphase Flow, Volume 158, 2023, 104299, ISSN 0301-9322. https://doi.org/10.1016/j.ijmultiphaseflow.2022.104299

[23] Hantao Jiang, Changshuang Zhi, Yingwen Liu. Thermal-hydraulic investigation of liquid metal cross flow different arrangements of tube bundles under pulsating flow. International Journal of Thermal Sciences, Volume 205, 2024, 109256, ISSN 1290-0729. https://doi.org/10.1016/j.ijthermalsci.2024.109256

[24] Hantao Jiang, Wenqiang Suo, Yingwen Liu. Analysis of flow structure of liquid metal pulsating cross flow in-line tube bundles with various pitch-to-diameter ratio. European Journal of Mechanics - B/Fluids, 2025, 204259, ISSN 0997-7546. https://doi.org/10.1016/j.euromechflu.2025.204259

[25] Songzhen Tang, Liang Ding, Ranran Sheng, Kai Zhao, Dongwei Zhang, Bo Shen. Parametric analysis on thermal-hydraulic characteristics in variable-direction twisted-oval tube bundle in crossflow. International Journal of Thermal Sciences, Volume 197, 2024, 108761, ISSN 1290-0729. https://doi.org/10.1016/j.ijthermalsci.2023.108761

[26] Junjie Zhou, Xinyu Xie, Songzhen Tang, Yanyan Xu, Xiuzhen Li. Numerical investigation and comparison on thermal-hydraulic performance of H-type finned tube heat exchanger. Case Studies in Thermal Engineering, Volume 59, 2024, 104481, ISSN 2214-157X. https://doi.org/10.1016/j.csite.2024.104481

[27] A. Žkauskas.(1987). Heat Transfer from Tubes in Crossflow. Editor(s):James P. Hartnett, Thomas F. Irvine. Advances in Heat Transfer, Elsevier, Volume 18, 1987, Pages 87-159, ISSN 0065-2717, ISBN 9780120200184. https://doi.org/10.1016/S0065-2717(08)70118-7

[28] H. K. Versteeg and W. Malalasekera. (2007). An Introduction to Computational Fluid Dynamics. ISBN: 978-0-13-127498-3.

[29] Çengel, Y.A., Ghajar, A.J., Heat and Mass Transfer: Fundamentals and Applications. McGraw-Hill Education. ISBN: 978-0-07-107786-6